



# Laser recovery of machining damage under curved silicon surface

Jiawang Yan <sup>a,\*</sup>, Fuminori Kobayashi <sup>b</sup>

<sup>a</sup> Department of Mechanical Engineering, Faculty of Science and Technology, Keio University, Hiyoshi 3-14-1, Kohoku-ku, Yokohama 223-8522, Japan

<sup>b</sup> Department of Mechanical Systems and Design, Graduate School of Engineering, Tohoku University, Aoba 6-6-01, Aramaki, Aoba-ku, Sendai 980-8579, Japan

Submitted by Takahisa Masuzawa (1).

## ARTICLE INFO

### Keywords:

Surface integrity  
Single crystal  
Laser recovery

## ABSTRACT

Nano-second pulsed laser irradiation was used to recover machining-induced damage under curved surfaces of single-crystal silicon. Microstructural changes of silicon due to laser irradiation were characterized by cross-sectional transmission electron microscopy and laser micro-Raman spectroscopy. The recoverable damage depth was predicted by finite element modeling of laser-induced temperature change in the workpiece material. Slanted irradiation experiments were performed and the critical surface inclination angle for complete recovery was experimentally obtained. The results demonstrate that atomic-level subsurface integrity and nanometric surface roughness can be achieved on large-curvature silicon surfaces, such as the surfaces of toroidally shaped wafer edges.

© 2013 CIRP.

## 1. Introduction

Manufacturing of defect-free silicon component is indispensable for production of dark-field optics, optoelectronic elements, and micro electromechanical systems [1]. Conventionally, silicon is machined by slicing, cutting, grinding and lapping, and then the machining-induced subsurface damage is removed by chemical etching and chemo-mechanical polishing. Due to the uncertainty of chemical reaction and the elasticity of polishing tools, it is difficult to precisely control local material removal depth. For this reason, it is extremely difficult to guarantee the form accuracy of workpiece having curved and micro-structured surfaces which are required more and more in current industries.

In this study, pulsed laser irradiation is used to recover the machining damage under curved silicon surfaces. Differently from conventional laser processes, the laser recovery process involves rapid top-down melting and bottom-up crystal regrowth of the damaged layer, yielding atomic-level subsurface integrity. In this paper, laser-induced temperature change and material structural change were investigated for slanted and curved silicon surfaces. The results demonstrate that the laser recovery technique can be used to generate completely defect-free surfaces on curved and micro-structured workpieces of single-crystal silicon.

## 2. Process modeling

### 2.1. Laser recovery mechanism

Typically, precision machining-induced subsurface damage of silicon includes an amorphous layer (a few tens of nanometers in thickness) and dislocations/microcracks (a few submicrons in depth) under the amorphous layer [2,3]. The proposed laser recovery mechanism is schematically shown in Fig. 1. Since

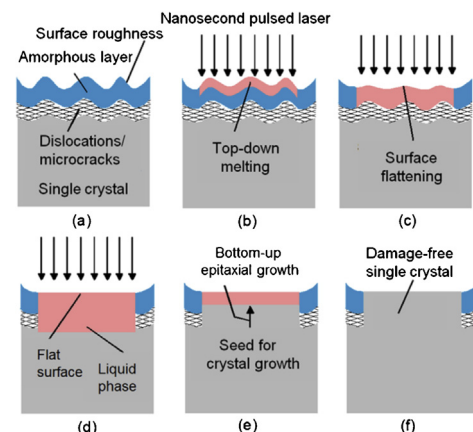


Fig. 1. Schematic diagram of laser recovery mechanism.

amorphous silicon has a remarkably higher laser absorption rate than crystalline silicon, there is sufficient absorption of laser in the near-surface layer to form a liquid thin film (b). The liquid layer has a much higher absorption rate, thus becomes thicker and thicker (c). The top-down melted liquid phase finally extends below the dislocations/microcracks (d). After the laser pulse, environmental cooling results in bottom-up epitaxial growth from the defect-free bulk region which serves as a seed for crystal growth (e). In this way, a perfect single-crystal structure identical to the bulk region will be obtained (f). Moreover, due to the surface tension effect of the liquid layer during silicon melting, an initially rough surface may become smooth after crystal regrowth (b)–(f). Therefore, improvement in both surface quality and subsurface integrity may be realized at the same time.

The key point in this technique is that the defect-free crystalline bulk region serves as a seed for the bottom-up epitaxial regrowth [4]. This makes laser recovery process different from other laser

\* Corresponding author. Tel.: +81-45-566-1445; fax: +81-45-566-1495.  
E-mail address: [yan@mech.keio.ac.jp](mailto:yan@mech.keio.ac.jp) (J. Yan).

processing techniques such as laser polishing/machining [5–7], laser melting [8] and laser annealing [9]. For example, in laser annealing, laser is used to crystallize sputtered, ion-implanted or vapor-deposited amorphous silicon thin films on substrates of glass, sapphire, etc., where no lattice-matched crystal seed exists. As a result, poly-crystal structures are formed.

2.2. FEM analysis of laser-induced temperature change

In laser recovery, it is essential to make the depth of melted workpiece material larger than that of the deepest dislocations and microcracks. To establish the relationship between melted depth and laser power, finite element method (FEM) analysis of laser-induced temperature change was performed using Comsol Multiphysics software. Fig. 2 shows an FEM model we used, which is composed of a thin amorphous layer (a-Si) on crystalline bulk (c-Si). Different thermal and optical properties were given to a-Si, c-Si, and liquid silicon according to literature [10]. The equations for laser intensity attenuation with laser penetration depth are given in Fig. 2, where  $I$  is laser intensity,  $z$  penetration depth,  $d_a$  thickness of a-Si (50 nm in this case),  $R$  reflection coefficient, and  $\alpha$  absorption coefficient (determined by laser wavelength  $\lambda$  and extinction coefficient  $\kappa$  [10]). The subscripts  $a$  and  $c$  refer to a-Si and c-Si, respectively. The function of heat conduction is also given in Fig. 2, where  $\rho$  is density,  $C_p$  specific heat,  $T$  temperature,  $t$  time,  $k$  heat conduction coefficient, and  $Q$  quantity of heat.

An example of simulated temperature change with time during a single laser pulse is shown in Fig. 3. Right after the laser pulse is irradiated on the surface, surface temperature rises sharply (b) and the high-temperature region extends rapidly downward into the

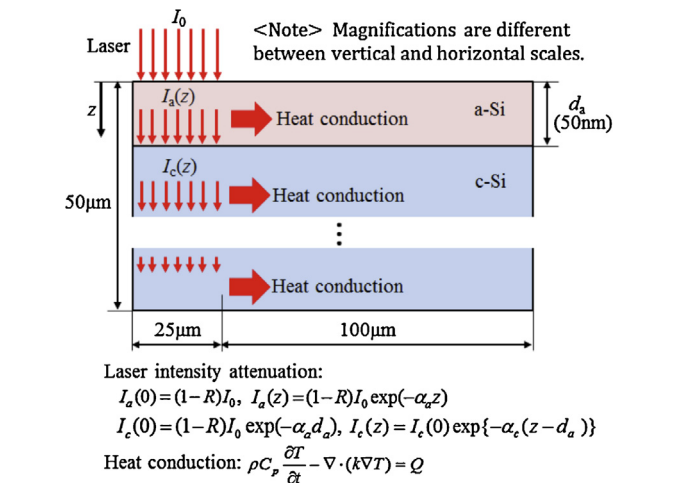


Fig. 2. FEM model for laser-induced temperature change.

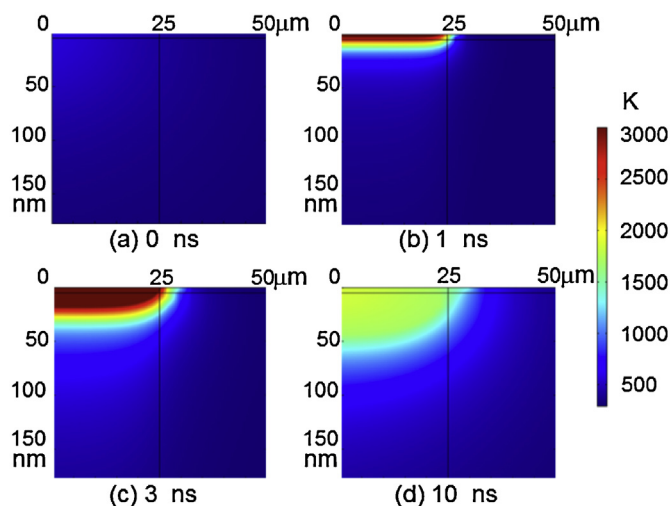


Fig. 3. FEM simulated temperature change during a laser pulse.

bulk region (c). Then after the laser pulse, heat keeps to transfer to surrounding regions, causing the temperature of the near-surface layer decrease gradually (d). It is this kind of heating-cooling cycle that enables the top-down melting and bottom-up crystal growth shown in Fig. 1. Fig. 4 shows temperature changes at different depths (0–250 nm) from the surface at various laser energy densities. It can be seen that the depth of melted region, where temperature is higher than the melting point of a-Si ( $T_{a-Si}$ , 1420 K) and c-Si ( $T_{c-Si}$ , 1688 K), is strongly dependent on laser energy density. In Fig. 4(a), where laser energy density is 0.10 J/cm<sup>2</sup>, only a thin layer of a-Si (<50 nm) can be melted. In Fig. 4(b), however, the c-Si region at a depth of 150 nm can be melted. Then in Fig. 4(c), where laser energy density is 0.65 J/cm<sup>2</sup>, the melted depth becomes larger than 250 nm. The FEM simulation assists selection of laser power for recovering damage at various depths.

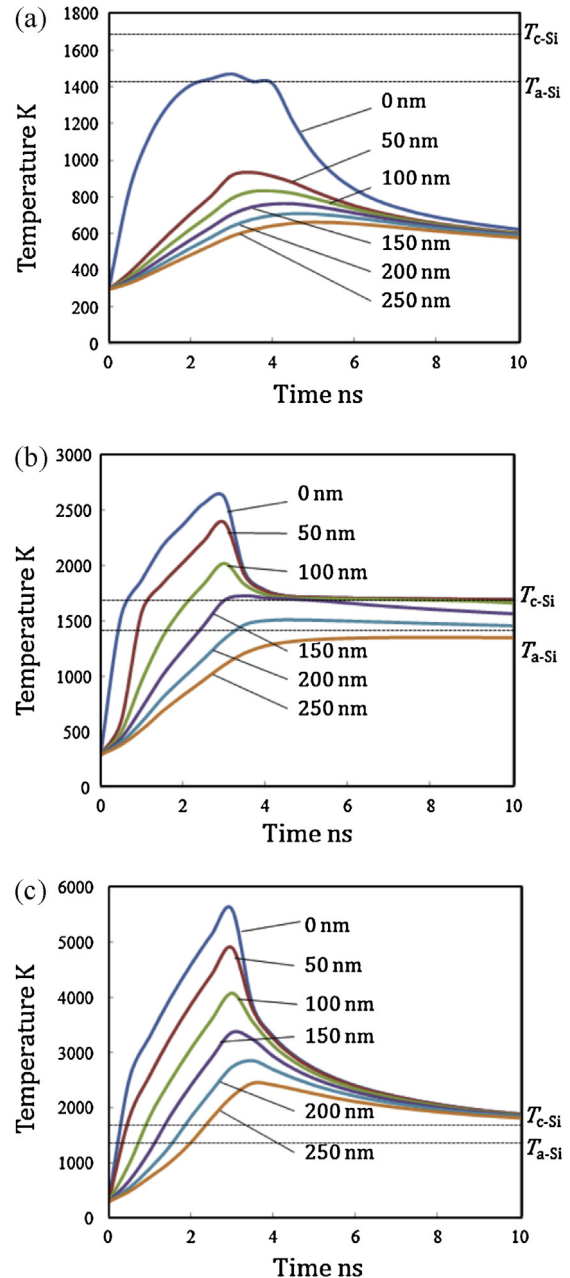


Fig. 4. Temperature changes at various depths from surface at different laser energy densities: (a) 0.10 J/cm<sup>2</sup>, (b) 0.30 J/cm<sup>2</sup> and (c) 0.65 J/cm<sup>2</sup>.

3. Experiments

Laser recovery tests were carried out using a laser system which employs a flash lamp-pumped Nd:YAG rod in a thermally compensated three bar invar resonator to generate radiation at

1064 nm. The 1064 nm laser pulse passes through an angle-tuned KTP crystal and generates the second harmonic at 532 nm. The second harmonic was selected because the penetration depth of laser light at this wavelength is 70 nm into a-Si and 1 μm into c-Si, which matches the depth range of machining damage. The laser pulse duration is 3–4 ns. The laser beam was shaped to a square section of ~50 μm × 50 μm using XY apertures. The laser oscillator was mounted onto a specially developed four-axis (XYZθ) numerical controlled precision stage made of ceramics. The XY tables of the stage were driven by linear motors on air slides and feedback-controlled by linear scales with a resolution of 0.1 μm.

Silicon wafers prepared by diamond grinding (abrasive grain size 2–4 μm) were used as workpiece. Laser irradiation was performed on both the flat surfaces and the curved edges of the wafers. In order to examine the microstructural changes caused by laser irradiation, a laser micro-Raman spectrometer, JASCO NRS-3100, and a transmission electron microscope (TEM), Hitachi HF2000, were used to characterize the samples. The ion milling technique was used to prepare the TEM samples.

### 4. Results and discussion

#### 4.1. Effect of laser energy density

Firstly, the laser beam was perpendicularly irradiated on a flat surface of a silicon wafer to investigate the effect of laser energy density. Fig. 5(a) is a cross-sectional TEM micrograph of a sample before laser irradiation. Grinding-induced damage involving an amorphous layer (depth ~50 nm) and dislocations (depth ~200 nm) can be clearly identified. Fig. 5(b) is a TEM micrograph of a sample irradiated at laser energy density of 0.30 J/cm<sup>2</sup>. A residual dislocation is observed under the surface although the damage in adjacent region has been almost recovered. This result indicates that laser energy density in this case is sufficiently high to melt the near-surface amorphous layer but too low to melt the dislocation in a deeper region (~200 nm). As a result, the residual dislocation grows up to the surface during the bottom-up crystal

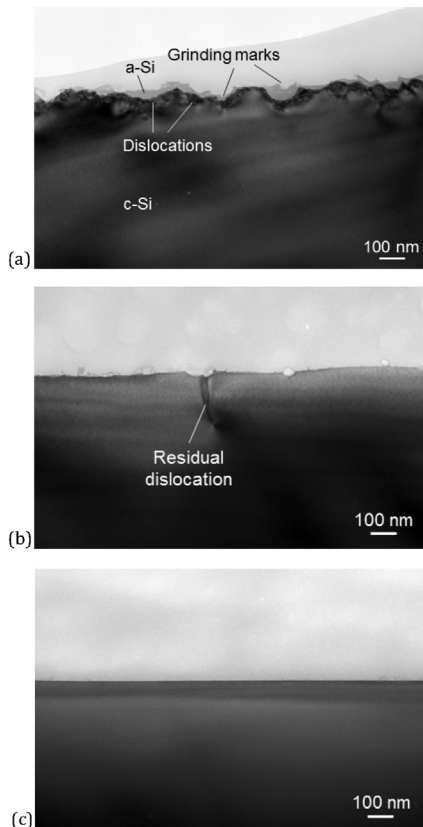


Fig. 5. Cross sectional TEM micrographs of (a) unirradiated surface and laser irradiated surface at energy densities of (b) 0.30 J/cm<sup>2</sup> and (c) 0.65 J/cm<sup>2</sup>.

growth. However, at laser energy density of 0.65 J/cm<sup>2</sup> (Fig. 5(c)), the subsurface damage has been completely recovered. These results agree with the FEM simulation results in Section 2.2.

#### 4.2. Effect of surface inclination angle

Laser reflection ratio and laser energy density distribution on a surface will change with the inclination angle and curvature of the surface. Next, the laser beam was inclined at various angles to the wafer surface to investigate effect of surface inclination on subsurface damage recovery. Fig. 6 shows Nomarski micrographs of laser-irradiated samples and plots of Raman intensity ratio (*r*) which is an indication of crystallinity [11]. A slight color change is seen after laser irradiation and the shape of irradiated region changes from a square (a) to trapezoids (b)–(d) due to laser beam broadening when the beam is slanted. The measurement of Raman intensity ratio *r* was performed across the laser irradiated regions as indicated by the arrows in the micrographs. When the inclination angle is lower than 45°, *r* is high (~0.9) and constant, indicating that the a-Si layer has been completely transformed into single crystal. However, at the 60° inclination angle, as shown in Fig. 6(d), *r* drops gradually at the lower region, indicating that

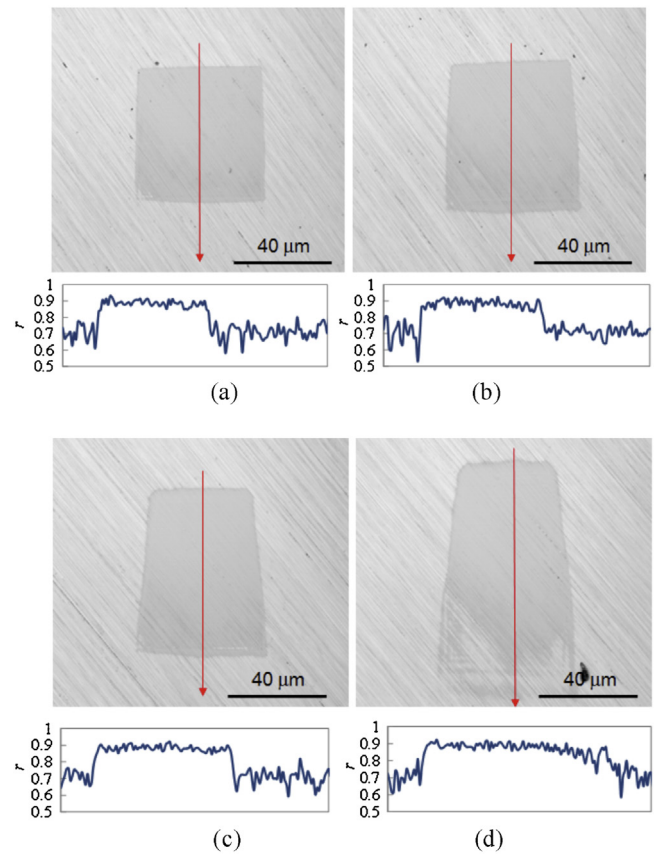


Fig. 6. Surface micrographs and plots of Raman intensity ratio at inclination angle of (a) 15°, (b) 30°, (c) 45° and (d) 60°.

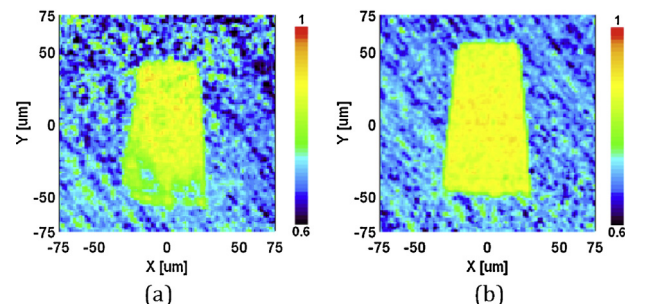


Fig. 7. Raman mapping of surfaces irradiated at an inclination angle of 60° and energy densities of (a) 0.30 J/cm<sup>2</sup> and (b) 0.65 J/cm<sup>2</sup>.

damage recovery in this region is incomplete. This result indicates that surface inclination should be controlled below a certain critical angle for recovering curved surfaces. Otherwise, a higher laser energy density will be required. Fig. 7 shows Raman intensity ratio mapping of surfaces irradiated at 60° inclination angle and different laser energy densities. In Fig. 7(a), the lower part of the irradiated region remains unrecovered, whereas in Fig. 7(b), the entire region was uniformly recovered.

#### 4.3. Laser recovery of large-curvature surface

Finally, laser irradiation was performed on silicon wafer edges to investigate the laser recovery characteristics of large-curvature surfaces. Fig. 8 schematically shows the cross section of a wafer edge, which has a toroidal surface with varying curvatures. In this study, the laser beam was directed to the edge surface from three directions using a specially developed laser scanning system, where surface inclination angle is controlled to be smaller than the critical angle. Fig. 9 shows micrographs of a laser irradiated wafer edge. After laser irradiation, grinding marks and micro pits disappeared and the surface became distinctly smoother.

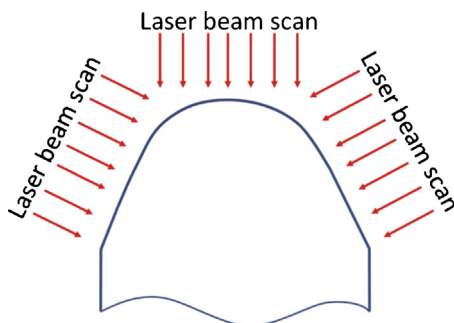


Fig. 8. Cross sectional profile of silicon wafer edge.

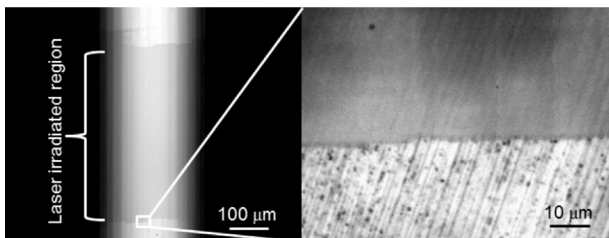


Fig. 9. Micrographs of laser-recovered region on wafer edge.

Fig. 10 is a cross-sectional TEM micrograph of the boundary between irradiated and unirradiated regions. In the unirradiated region, under diamond-ground surface, there is an amorphous layer below which are dislocations. In the laser irradiated region, however, both the amorphous layer and the dislocations were not observed. A perfect single-crystal structure identical to that of the bulk material has been achieved. From the TEM result, we can also

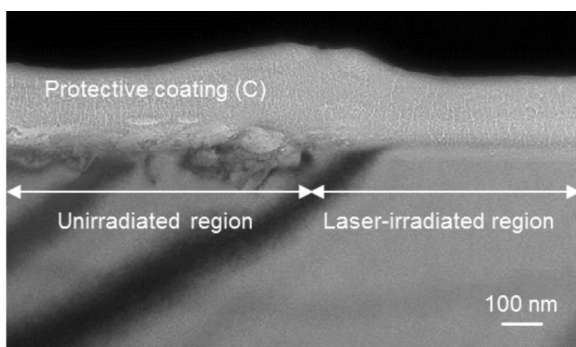


Fig. 10. Cross sectional TEM micrograph of silicon wafer edge before/after laser recovery.

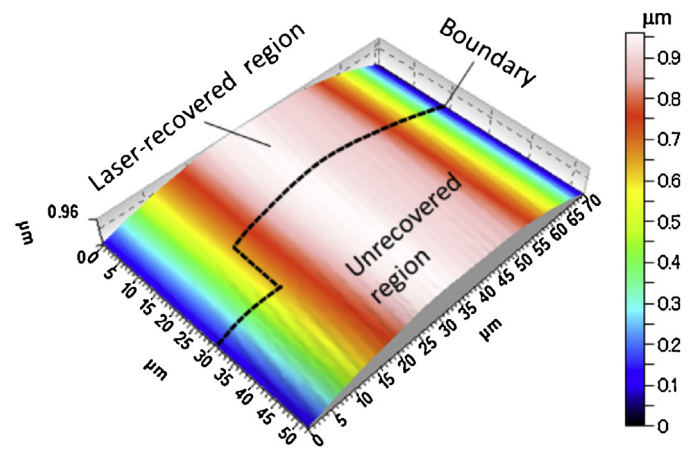


Fig. 11. Three dimensional surface topography of silicon wafer edge before/after laser recovery.

see that the surface became remarkably smooth after laser recovery. Fig. 11 is a three dimensional surface topography of the wafer edge. The surface roughness after laser recovery is ~2 nm Ra, demonstrating that atomic-level subsurface integrity and nanometric surface roughness were achieved at the same time.

## 5. Conclusions

Nano-second pulsed laser was used to recover grinding-induced damage in silicon. The recoverable damage depth was predicted by FEM simulation. Laser recovery tests of slanted and curved surfaces were performed and the critical conditions for complete recovery were experimentally found. The results demonstrate that atomic-level subsurface integrity and nanometric surface roughness can be achieved on large-curvature toroidally shaped silicon surfaces by laser recovery. This process involves no material removal, no emission and no pollution, thus provides an effective new approach for ultraprecision manufacturing.

## References

- [1] Lucca DA, Brinksmeier E, Goch G (1998) Progress in Assessing Surface and Subsurface Integrity. *Annals of the CIRP* 47(2):669–693.
- [2] Puttick KE, Whitmore LC, Chao CL, Gee AE (1994) Transmission Electron Microscopy of Nanomachined Silicon Crystals. *Philosophical Magazine A* 69(1):91–103.
- [3] Yan J, Asami T, Harada H, Kuriyagawa T (2012) Crystallographic Effect on Subsurface Damage Formation in Silicon Microcutting. *Annals of the CIRP* 61(1):131–134.
- [4] Yan J, Asami T, Kuriyagawa T (2007) Response of Machining-damaged Single-crystalline Silicon Wafers to Nanosecond Pulsed Laser Irradiation. *Semiconductor Science and Technology* 22:392–395.
- [5] Olsen FO, Alting L (1995) Pulsed Laser Materials Processing, Nd–YAG versus CO<sub>2</sub> Lasers. *Annals of the CIRP* 44(1):141–145.
- [6] Meijer J, Du K, Gillner A, Hoffmann D, Kovalenko VS, Masuzawa T, Ostendorf A, Poprawe R, Schulz W (2002) Laser Machining by Short and Ultrashort Pulses, State of the Art and New Opportunities in the Age of the Photons. *Annals of the CIRP* 51(2):531–550.
- [7] Li L, Hong M, Schmidt M, Zhong M, Malshe A, Huis in't Veld B, Kovalenko V (2011) Laser Nano-manufacturing – State of the Art and Challenges. *Annals of the CIRP* 60(2):735–755.
- [8] Brinksmeier E, Levy G, Meyer D, Spierings AB (2010) Surface Integrity of Selective-laser-Melted Components. *Annals of the CIRP* 59(1):601–606.
- [9] André G, Bergmann J, Falk F (2005) Laser Crystallized Multicrystalline Silicon Thin Films on Glass. *Thin Solid Films* 487(1–2):77–80.
- [10] Palik ED (1985) *Handbook of Optical Constants of Solids*, Academic Press, Orlando.
- [11] Yan J, Asami T, Kuriyagawa T (2008) Nondestructive Measurement of the Machining-induced Amorphous Layers in Single-crystal Silicon by Laser Micro-Raman Spectroscopy. *Precision Engineering* 32(3):186–195.